

Probing Sub-Micron Forces by Interferometry of Bose-Einstein Condensed Atoms

Savas Dimopoulos* and Andrew A. Geraci†

Department of Physics, Stanford University, Stanford, CA 94305

(Dated: May 22, 2019)

Abstract

We propose a technique, using interferometry of Bose-Einstein condensed alkali atoms, for the detection of sub-micron-range forces. It may extend present searches at 1 micron by 6 to 9 orders of magnitude, deep into the theoretically interesting regime of 1000 times gravity. We give several examples of both four-dimensional particles (moduli), as well as higher-dimensional particles – vectors and scalars in a large bulk– that could mediate forces accessible by this technique.

PACS numbers: 04.50.+h, 04.80.Cc, 11.25.Wx

*savas@stanford.edu

†aageraci@stanford.edu

I. INTRODUCTION

Some recent theoretical ideas point to the possibility of new physics, related to gravity, at the sub-millimeter regime. One is the preponderance of light gravitationally coupled moduli suggested by string theory [1, 2]. Another is the possibility of large sub-mm-size dimensions and the particles residing inside its bulk [3, 4, 5]. Yet another is suggested by the magnitude of the vacuum energy [6].

These ideas motivated some heroic experiments [7, 8, 9, 10, 11] that have, in the last seven years, extended the search for such forces from mm down to ~ 20 microns. These experiments involve measuring the force between two macroscopic but small objects. A fundamental obstacle in searching at much smaller distances is that the size of these objects must be reduced and therefore the expected signal force decreases; at the same time, the electrostatic background Van-der-Waals force increases.

In this paper we suggest a possible way around this obstacle by considering the interaction of a macroscopic system with a pure quantum mechanical system consisting of a Bose-Einstein condensate. The latter has a significant advantage relative to a macroscopic system: its de Broglie phase can be measured very precisely. In addition, it can be well controlled and manipulated and its electromagnetic interaction with its environment is well understood – both theoretically and experimentally. Because of these advantages, the technique that we propose may extend current bounds at 1 micron by 6 to 9 orders of magnitude, and be sensitive to forces as small as 1000 times gravity. The approach we describe thus explores a region of parameter space that is complementary to the super-micron reach of upcoming micro-cantilever and torsion balance experiments.

In section 2 we update the analysis of macroscopic forces below 10 microns in theories with light moduli. In section 3 we consider new forces from bulk gauge fields or scalars in large extra dimensions, taking baryon number as an example. In section 4 we propose our experimental technique and estimate some of the important backgrounds. We conclude with section 5.

II. FORCES FROM LIGHT MODULI

In string theory the parameters of the standard model depend on fields, called moduli, whose values determine the geometry of the extra dimensions. Moduli couple with gravitational strength and typically remain massless until supersymmetry is broken. So, they get a mass proportional to $\sim F/M_{\text{PL}}$, where F is the scale where supersymmetry breaking originates. In theories with gravity-mediated supersymmetry breaking, F is $(10^8 \text{ TeV})^2$ and the moduli have microscopic Compton wavelengths. However, as pointed out in reference [1], in theories of gauge-mediated supersymmetry breaking, F can be as small as $(10 \text{ TeV})^2$ and moduli can have macroscopic Compton wavelengths and mediate macroscopic forces of gravitational strength. The range and magnitude of these forces, for a variety of moduli, were first estimated in reference [1] for \sqrt{F} in the range of 10 TeV to 100 TeV. At that time it seemed pointless to consider larger values of F , since they lead to moduli Compton wavelengths which were thought to be inaccessible to macroscopic-force experiments. In this paper we extend the scale of \sqrt{F} up to 2000 TeV, which in turn considerably extends the predicted parameter space for moduli-dependent forces.

The upper limit for the value of \sqrt{F} comes from cosmology: In gauge-mediated supersymmetry breaking, the gravitino is the lightest supersymmetric particle, with mass $\sim F/M_{\text{PL}}$. Although light, its mass still must not exceed 1 keV to avoid over-closing the universe [12]. This in turn provides an upper limit of 2000 TeV on \sqrt{F} .

We focus on the three classes of moduli studied in reference [1] which couple directly to ordinary matter: the dilaton, the gauge moduli and the Yukawa moduli. Moduli-dependent forces can occupy a substantially larger region of parameter space than previously indicated. Although much recent experimental progress has been made in the search for new sub-millimeter forces [11],[13] there is ample potentially interesting parameter space awaiting further exploration.

A. Gluon modulus

We consider here a field ϕ that couples only to the standard model gluons. The effective coupling is given by [1]

$$\mathcal{L} = \frac{\lambda_g}{8\pi^2 M} \frac{\phi}{M} G_{\mu\nu}^a G^{a\mu\nu}, \quad (1)$$

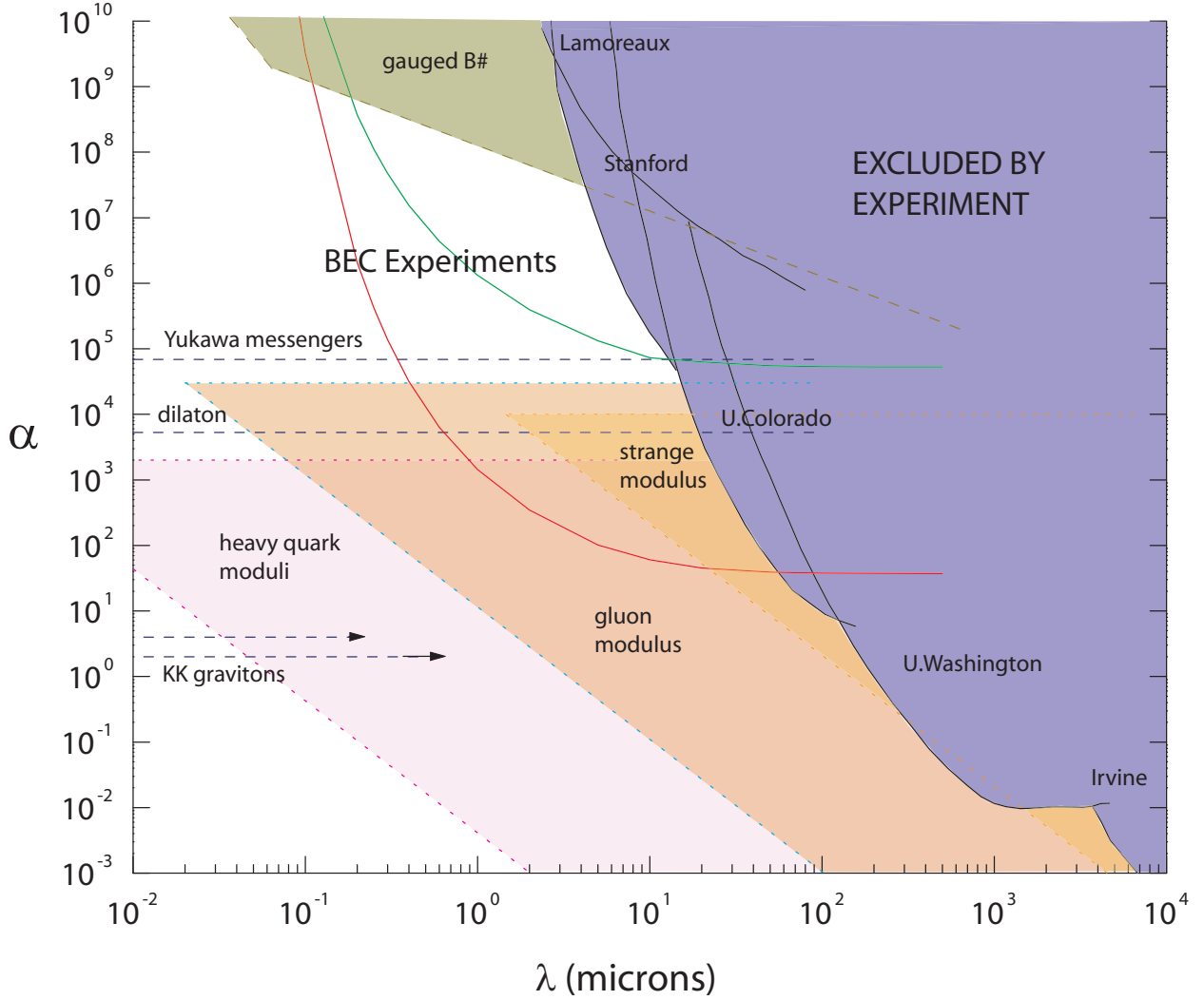


FIG. 1: Experimental bounds and theoretical expectations on new forces from potentials of the form $V(r) = -G_N \frac{m_1 m_2}{r} (1 + \alpha e^{-r/\lambda})$ below 1 cm. The projected reach of the first-round BEC experiments is shown as a solid green line. The solid-red line indicates the reach with an improved sensitivity of 10^{-7} Hz. Experimental data are from references [8, 9, 10, 14, 15]. The shown theoretical expectations are discussed in the text.

where λ_g is an undetermined coupling constant, M is expected to be of the order of the string scale 5×10^{17} GeV, and the suppression factor $8\pi^2$ accounts for the gauge coupling depending on moduli only at higher-order. In this way, the coupling strength is weaker than that of the dilaton discussed in the following subsection.

Considering the contribution to its mass coming from the interaction in eq. (1), the

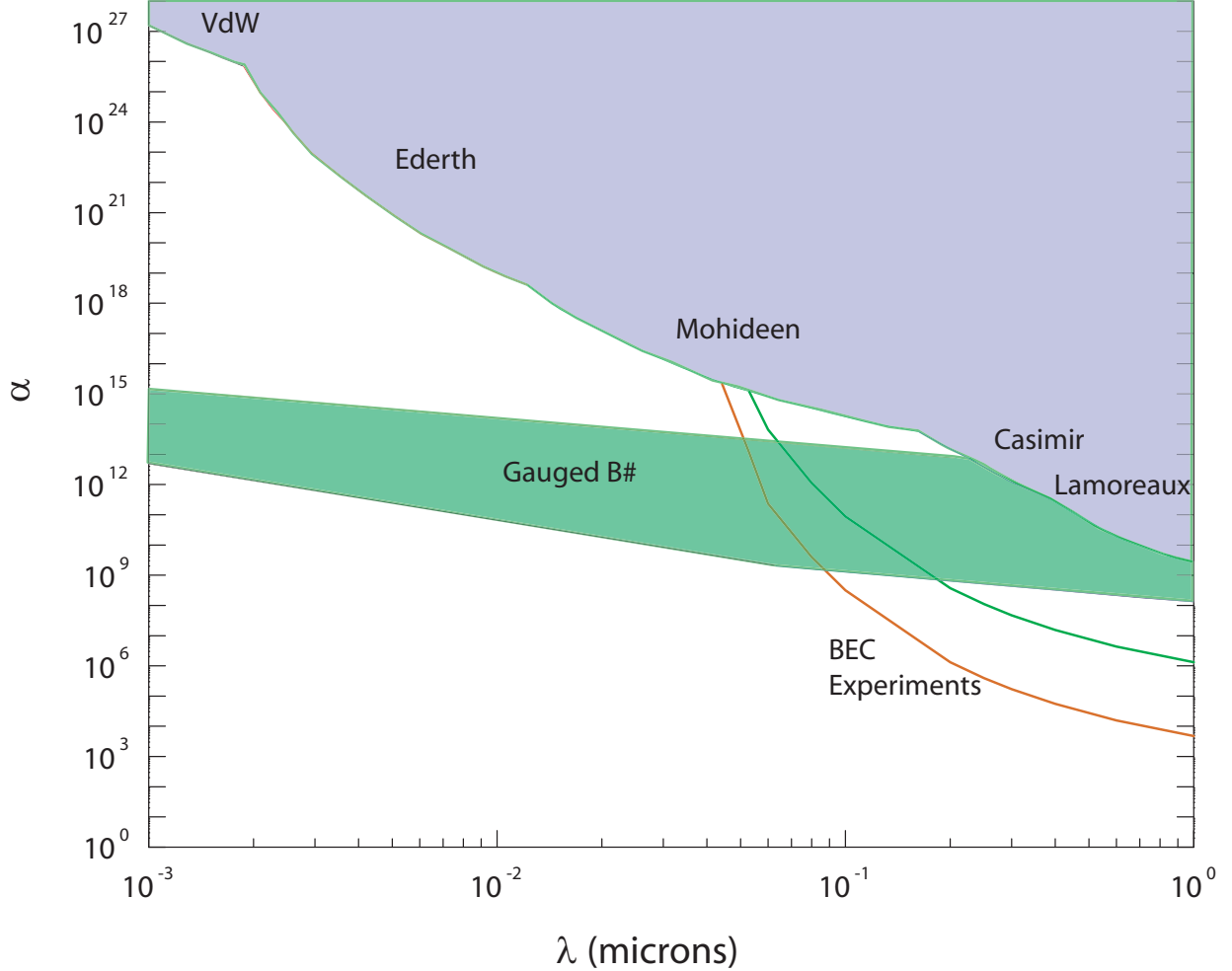


FIG. 2: Experimental bounds on new forces from potentials of the form $V(r) = -G_N \frac{m_1 m_2}{r} (1 + \alpha e^{-r/\lambda})$ below 1 micron. The projected reach of the first-round BEC experiments is shown as a solid green line. The solid-red line indicates the reach with an improved sensitivity of 10^{-7}Hz . Experimental data are adapted from a figure in reference [13]

Compton wavelength of the field is [1]

$$\lambda_\phi = 8 \times 10^{-4} \text{ m} \lambda_g^{-1} \left(\frac{M}{5 \times 10^{17} \text{ GeV}} \right) \frac{(100 \text{ TeV})^2}{F} (kN)^{-1/2} . \quad (2)$$

Here F is the fermion-scalar messenger mass-squared splitting, k is a loop-integral factor of order 1, and N is the number of messenger multiplets. $N < 4$ is required so that all gauge couplings remain perturbative below the GUT scale, and a bound of $\sqrt{F} > 30 \text{ TeV} / \sqrt{N}$ can be imposed from constraints on the right-handed selectron mass and a consistency condition that the messengers have non-negative mass-squared [1].

The coupling of ϕ to the nucleon N can be expressed by

$$\mathcal{L} = \mathcal{G}_\phi \frac{m_N}{M_{\text{PL}}} \phi \bar{\psi}_N \psi_N , \quad (3)$$

where \mathcal{G}_ϕ is given by

$$\mathcal{G}_\phi = \frac{\lambda_g}{8\pi^2} \frac{M_{\text{PL}}}{M} \frac{\langle N | G_{\mu\nu}^a G^{a\mu\nu} | N \rangle}{m_N} \simeq -6 \lambda_g \left(\frac{5 \times 10^{17} \text{ GeV}}{M} \right) . \quad (4)$$

The interaction in eq. (3) yields a potential for ϕ exchange between particles of mass m_1 and m_2 at a distance r :

$$V(r) = G_N m_1 m_2 \mathcal{G}_\phi^2 \int \frac{d^3 k}{(2\pi)^3} \frac{e^{i\vec{k}\cdot\vec{r}}}{\vec{k}^2 + m_\phi^2} . \quad (5)$$

When added to gravity, eq. (5) describes an additional attractive force:

$$V(r) = -G_N \frac{m_1 m_2}{r} \left(1 + \alpha e^{-r/\lambda_\phi} \right) , \quad (6)$$

where α is given by $\mathcal{G}_\phi^2/4\pi$. In reference [1], a range of λ_{ϕ_g} and α was obtained by taking $\sqrt{k}N = 1$ and by varying \sqrt{F} between 30 and 100 TeV and $\lambda_g^{-1} \times M/(5 \times 10^{17} \text{ GeV})$ between 10^{-2} and 10^2 . We here expand the range for the SUSY scale \sqrt{F} up to the limit of 2000 TeV imposed by the gravitino problem and show the results in Figure 1.

B. Dilaton

The dilaton couples to nucleons with a strength of about 80 times gravity [1, 16, 17], leading to an inter-nucleon force of about 6400 times gravity. Since it couples to all fields in the theory, it is expected to receive a mass $\sim F/M$ from its strong coupling to the primordial supersymmetry-breaking sector. This would make its Compton wavelength less than $10^{-2} \mu\text{m}$ $(100 \text{ TeV})^2/F$, which is too short to be experimentally observed. However, as Damour and Polyakov speculate [18], since the dilaton potential is related to the cosmological constant, the yet unknown mechanism accounting for the smallness of the cosmological constant may also make the dilaton light. Since there is no good theory of the dilaton mass, the line labelled "dilaton" in Figure 1 should be terminated a point determined by experiment.

C. Yukawa moduli

The Yukawa couplings of the standard model could also depend on moduli which are relatively unaffected by Planck scale physics, but obtain a mass due to (low-scale) supersymmetry breaking [1]. A Yukawa modulus ϕ may be coupled as follows to up-type quarks and the Higgs boson H :

$$\mathcal{L} = \lambda(\phi) q_L \bar{u}_R H_u + \text{h.c.} , \quad (7)$$

along with analogous terms for down-type quarks and charged leptons. Here flavor indices have been suppressed and we for simplicity assume one modulus per coupling.

Yukawa terms of the form in eq. (7) contribute to an effective potential for ϕ :

$$V(\phi) = \frac{8kN\alpha_s^2}{3(16\pi^2)^3} \lambda^\dagger(\phi) \lambda(\phi) F^2 + V_0(\phi)$$

where again F is the fermion-scalar messenger mass-squared splitting, k is a loop-integral factor of order 1, N is the number of messenger multiplets, and V_0 describes any additional unknown contribution to the potential not due to the operator in eq. (7). The coupling can be expanded around its minimum $\langle\phi\rangle \sim M$, where M is of order string scale,

$$\lambda(\phi) = \lambda^{(0)} + \lambda^{(1)} \frac{(\phi - \langle\phi\rangle)}{M} + \frac{1}{2} \lambda^{(2)} \frac{(\phi - \langle\phi\rangle)^2}{M^2} + \dots$$

and a lower bound on the modulus mass can be obtained from the known term in

$$m_\phi^2 = \frac{16kN\alpha_s^2}{3(16\pi^2)^3} (\lambda^{(1)2} + \lambda^{(0)}\lambda^{(2)}) \frac{F^2}{M^2} + \frac{d^2V_0}{d\phi^2} |_{\phi = \langle\phi\rangle}.$$

For a particular flavor modulus, the coupling $\lambda^{(0)} = 2m_q/\sqrt{2}vH_q$ where v is the Higgs vacuum expectation value of 246 GeV, and H_q equals $\sin\beta$ for up-type quarks and $\cos\beta$ for down-type, where $\tan\beta$ is the ratio of the Higgs' vacuum expectation values. Using this result, the Compton wavelength becomes

$$\begin{aligned} \lambda_\phi &= 1050\mu m \times \alpha_s^{-1} \frac{F}{(100\text{TeV})^2} \frac{5 \times 10^{17}\text{GeV}}{M} \\ &\times \left(\frac{\text{GeV}}{m_q} \right) \left(\frac{H_q}{\frac{1}{\sqrt{2}}} \right) \left[\left(\frac{\lambda^{(1)2}}{\lambda^{(0)2}} + \frac{\lambda^{(2)}}{\lambda^{(0)}} \right) kN \right]^{-1/2}. \end{aligned}$$

We arrive at an expression larger than reported previously in reference [1] due to a corrected numerical factor.

The long-range force potential can be determined by relating the scalar ϕ -quark coupling of eq. (7) to the scalar ϕ -nucleon coupling. The fields ϕ corresponding to up and down quarks can generally have different couplings to the proton and the neutron, leading to small violations of the equivalence principle. The scalar coupling of the field ϕ to the nucleon N is again expressed in terms of eq. (3) where

$$\mathcal{G}_\phi = \frac{\lambda^{(1)}}{\lambda^{(0)}} \frac{M_{\text{PL}}}{M} \frac{\langle N | m_q \bar{q} q | N \rangle}{m_N}. \quad (8)$$

The results for the Compton wavelengths and the strengths of the moduli forces relative to gravity are plotted in Figure 1. The areas are obtained by taking $kN = 1$, $\tan \beta = 1$, $\lambda^{(2)} = 0$, by varying \sqrt{F} between 30 and 2000 TeV, and by varying $\lambda^{(0)}/\lambda^{(1)} \times M/(5 \times 10^{17} \text{ GeV})$ between 10^{-2} and 10^2 .

III. FORCES FROM PARTICLES IN LARGE EXTRA DIMENSIONS

In theories with large extra spatial dimensions the fundamental scale M_* and the observed four-dimensional Planck scale $M_4 = 2.43 \times 10^{18} \text{ GeV}$ are related by

$$M_4^2 = M_*^{n+2} V_n$$

where n is the number of extra dimensions and V_n is their volume. In this framework, the standard model gauge and matter content is confined to a 4-dimensional submanifold, and the graviton can propagate in all $4 + n$ dimensions. The scenario provides an alternative solution to the gauge hierarchy problem [3, 4, 5], as the fundamental scale can be of order TeV. Such a paradigm also predicts a modification to Newton's law of gravitation at distances nearby and below the length-scale of compactification.

A. Gravitons in the Bulk

The modification of Newton's law of gravitation in theories with large extra spatial dimensions has been studied in some detail [19, 20]. For equal-size extra dimensions and toroidal compactification, the volume satisfies $V_n = (2\pi R)^n = L^n$, and we have [5]

$$R_n = 2 \times 10^{31/n-16} \text{ mm} \times \left(\frac{1 \text{ TeV}}{M_{4+n}} \right)^{1+2/n}$$

For the case of two equal extra dimensions (n=2), the radius of compactification is of order 1-millimeter for $M_{4+n} \sim \text{TeV}$. However for this case, astrophysical bounds require the fundamental scale M_{4+n} to be pushed above 1600 TeV [21]. At this scale the two equal-size radii are only 2.4 Å. Requiring such a high energy scale in turn necessitates more fine tuning for the framework to address the hierarchy problem. For the case of 3 extra dimensions M_{4+n} must exceed 60 TeV, and the radius becomes $\sim .05$ Å for equal-size dimensions. These limits are derived from Kaluza-Klein gravitons that would be gravitationally trapped and remain as a halo surrounding neutron stars [21]. The constraints come from neutron star heating via Kaluza-Klein graviton decays. Somewhat weaker limits are also obtained from EGRET gamma-ray flux measurements of nearby supernovae and neutron stars. Upcoming measurements planned with the GLAST satellite may improve bounds further or lead to a new discovery. Both sets of constraints are weakened if the dimensions are of unequal size, if there are additional fast decay channels such as other branes for the KK gravitons to decay into, or if graviton emission is suppressed as in reference [22].

From the four-dimensional point of view, the higher dimensional graviton with momentum in the extra dimensions appears as a massive particle, leading to a sum of Yukawa potentials from the tower of Kaluza-Klein (KK) modes in addition to the massless graviton potential. At distances of order R_n , only the lowest massive mode contributes significantly while the higher modes are exponentially suppressed. For distances $r \ll R_n$, many modes contribute and change the power law dependence of the force from the Newtonian $1/r^2$ to $1/r^{2+n}$. Corrections to the newtonian potential between two masses m_1 and m_2 are typically parameterized according to the form

$$V(r) = -G_N \frac{m_1 m_2}{r} (1 + \alpha e^{-r/\lambda})$$

where α and λ characterize the strength relative to gravity and range of the new force, respectively. For distances of order R_n or greater, the range λ is the inverse of the lightest KK mass and the strength α equals its degeneracy [19, 20]. At shorter distances, more massive KK modes contribute until eventually the power law behavior of the force changes. We adopt the convention of references [19, 20] and consider only the leading term corresponding to the lightest massive KK modes. For example in the cases of toroidal and spherical compactification [19]

$$V(r)_{\text{n-torus}} = -\frac{G_N m_1 m_2}{r} (1 + 2n_0 e^{(-r/R_0)})$$

$$V(r)_{\text{n-sphere}} = -\frac{G_N m_1 m_2}{r} (1 + (n+1)e^{(-\sqrt{n}r/R)})$$

for n_0 equal radii of size R_0 .

Due to the stringent astrophysical constraints on two- or three- equal sized large extra dimensions, and their even smaller size for $n > 3$, it is unlikely in this case that the KK gravitons can be observed at table-top experiments. However, we stress that these constraints strictly apply to the case of equal extra dimensions. If the extra dimensions are not of equal size, it is possible some of the dimensions may be large enough to be detected. To illustrate this we plot the cases in (α, λ) space for toroidal compactification with one or two large radii (amongst possibly many smaller radii).

B. Gauged Baryon Number in the Bulk

If in addition to the graviton there are bulk gauge particles, their effective four-dimensional gauge coupling g_4^2 can be many orders of magnitude stronger than gravity [5]. As a particular case we consider gauged baryon number B , with the gauge symmetry spontaneously broken only on a different submanifold than our own. As discussed in references [5, 23], such a situation can lead to an enormous suppression of the proton decay rate. In the following we systematically explore the parameter space for the force strength and range. Several details are deferred to the Appendix.

Since ordinary matter is primarily composed of baryons, the mass of a macroscopic object is roughly in proportion to the number of baryons, apart from small effects due to binding energy and the electron mass. The expected ratio of the gauge to gravitational forces will take the form

$$\alpha_g = \frac{F_{\text{gauge}}}{F_{\text{grav}}} = \frac{g_4^2}{4\pi G_N m_p^2} \quad (9)$$

where m_p is the mass of the proton. The effective four-dimensional gauge coupling is related to the massive $4+n$ -dimensional coupling by the volume of the extra dimensions

$$\frac{1}{g_4^2} = \frac{V_d}{g_{(4+n)}^2}.$$

We can express the $(4+n)$ dimensional coupling in terms of an ultraviolet cut-off scale for the gauge theory Λ which we expect to be of order M_* : $g_{4+n}^2 = \Lambda^{-n} \mathcal{O}_{4+n} \rho$, where $\mathcal{O}_d = \Omega_{(d-1)} / (2\pi)^d$ is the 1-loop suppression factor. If the coefficient ρ is $\mathcal{O}(1)$, this signifies

strong coupling in the $4+n$ dimensional theory, as loop effects become comparable to tree-level. Expressing the 4-dimensional coupling in eq. (9) in terms of $\Lambda \sim M_*$, we find the baryon-number force can easily reach strengths of $10^6 - 10^8$ times gravity, and even higher magnitude for strong-coupling with a large number of extra dimensions.

To avoid conflict with experiment, the baryon number gauge field must acquire a mass. If the gauge symmetry is spontaneously broken by a scalar field χ obtaining a vacuum expectation value $\langle \chi \rangle$, the resulting mass of a gauge particle A_μ becomes $m_A = g_4 \langle \chi \rangle$. Here again we assume that χ condenses on a brane other than our own. It was shown in reference [24] that forces mediated by bulk gauge fields can be exponentially weaker than gravity if the bulk gauge symmetry is spontaneously broken on our brane. For $\langle \chi \rangle = \beta M^*$ with β of $\mathcal{O}(1)$, the Compton wavelengths are in an interesting range for sub-millimeter experiments. A range of predicted parameter space is provided along with a more detailed analysis in the Appendix. A portion of the allowed phase space appears in Figures 1 and 2 for comparison with other sub-millimeter forces and experimental bounds.

Astrophysical bounds similar to those discussed for gravitons [5],[21],[25] can also apply for gauge particles in the bulk. In Supernova 1987A, about 10^{53} ergs of gravitational binding energy was released in a few seconds. One requirement is therefore that the total luminosity of Kaluza-Klein particles does not exceed $\sim 10^{53}$ erg s^{-1} . The temperature of the supernova is approximately $T \sim 30$ MeV, and most KK particles are produced with an energy of order ~ 100 MeV. The constraints on the total luminosity for KK gravitons imply $M_* > 30$ TeV for $n = 2$ extra dimensions [5]. For the case of gauge particles in the bulk, we expect the same amount of energy that would have gone into KK gravitons to now produce KK gauge bosons, producing roughly the same number of particles. However the rate of production for gravitons goes like T^n/M_*^{2+n} and for gauge bosons like T^{n-2}/M_*^n , which is more rapid. Therefore the constraints on the fundamental scale due to graviton emission for n extra dimensions apply for gauge particle emission with $n+2$ dimensions. A similar situation is discussed in reference [23] for the case of bulk scalars. This implies the more stringent limit of $M_* > \sim 30$ TeV for the case of $n = 4$ extra dimensions.

Neutron Star Limits. Kaluza-Klein excitations of the gauge bosons can also become gravitationally trapped and remain for some time in a cloud surrounding neutron stars. Their subsequent decays into photons can in certain cases produce observable gamma-ray signals detectable by EGRET. The decay width for such particles can be roughly computed

as

$$\Gamma = \frac{M_*^2 T}{M_{\text{Pl}}^2} , \quad (10)$$

where T is the temperature, typically of order 30 MeV for a supernova. The lifetime becomes $\sim 10 - 10000$ years for T from 1 GeV-1 MeV. (The decay width for gravitons goes as $\Gamma \sim T^3/M_{\text{Pl}}^2$, leading to lifetimes of order 6×10^9 years.) However, the situation can be quite different depending on the symmetry that is gauged. For $B - \zeta L$, where nonzero ζ denotes an admixture of lepton number, there are decay channels into neutrinos. In this case eq. (10) is a good approximation and the decays can occur on a time-scale of 10^2 years. Such a situation provides little direct observable gamma signal for EGRET. Also KK annihilation into positrons is possible, but the resulting gamma rays from positronium annihilation are of too low energy to be a useful EGRET source. In the case of pure B , where $\zeta = 0$, the lifetime given in eq. (10) has to be amended since the decay into photons occurs only at higher order. The decay width in this case is multiplied by an additional factor of $(\alpha/2\pi)^2$ due to a virtual fermion loop. This increases the lifetime by a factor of $\sim 10^6$, making it more comparable to the graviton case at $\sim 1.3 \times 10^8$ years. The resulting improvement in the bound on f_{KK} as compared with the graviton case is about 50 times. For bulk gauge particles, the bound on the compactification scale varies with f_{KK} as $M_{\text{min}} \propto (f_{KK})^{-1/n}$. In this situation, the bounds that applied for n extra dimensions in the graviton case now apply to $n + 2$ extra dimensions. We find the $n=4,5$ limits due to the neutron star gamma ray limits become roughly 3000 TeV and 60 TeV, respectively. Neutron star excess heat provides a limit of 11,000 TeV and 200 TeV, respectively. These sets of limits are due to neutron stars RX J185635-3754 and PSR J0953+0755 [21], both of which are younger than 10^8 years.

As was the case for graviton decays, the constraints may be weakened if the dimensions are of unequal size, or if there are additional fast decay channels such as "photons" on other branes for the KK particles to decay into.

C. Yukawa Messengers

An additional possibility is that scalar particles may inhabit the bulk of extra dimensions and mediate macroscopic forces, such as the Yukawa messengers considered in reference [23]. The messenger fields could be responsible for communicating flavor symmetry breaking from

other branes to our brane, and for example can attribute the weakness of light generation Yukawa couplings to geometrical power-law suppression or exponential suppression due to the mass of the messenger fields. In this framework, the vast variation in strengths of the Yukawa couplings is recast as a variation in distances to other branes. However, even if the messenger fields do not condense on our brane, they can still mediate forces much stronger than gravity. If the messenger fields acquire mass due to supersymmetry breaking on our wall, their Compton wavelength can be in the sub-millimeter range. As was the case with gauged baryon number, the coupling strength for such forces due to the zero mode can be large even if the extra dimensions are small enough to make the Kaluza-Klein modes too heavy to be detected in sub-millimeter experiments. The coupling strength $\rho \sim v/M_{\text{Pl}}$ where here v is the Higgs vacuum expectation value of 174 GeV and here M_{Pl} is the reduced Planck scale of 2.43×10^{18} GeV. Comparing to gravity, $\rho^2/(G_N m_{\text{nucleon}}^2) \sim 10^6$. As with the vectors described in the previous section, similar astrophysical constraints apply to the scalars in the bulk as discussed in reference [23].

IV. USING BOSE-EINSTEIN CONDENSED ATOMS TO PROBE (SUB)-MICRON DISTANCES

In recent years the field of atomic interferometry has produced a series of amazing measurements, including extremely high precision measurements of the acceleration due to the Earth's gravity at the level of a part per billion or better. These advances have been made possible due to the remarkable techniques developed for trapping and cooling alkali atoms (see, for example, the 1998 Nobel lectures of Chu, Cohen-Tannoudji, and Phillips [26]). Among recent experiments have been a series of atomic-fountain type measurements where an atomic beam is launched upwards and allowed to accumulate a phase shift in the Earth's gravitational field in a Mach-Zehnder-type interferometer configuration [27]. Similar experiments have also been carried out to perform sensitive measurements of gravity gradients [28]. Such precision techniques can also be used to measure large deviations from Newton's constant at short distances. Among the challenges of applying such systems to study gravity from nearby macroscopic objects is obtaining the optimized beam size and divergence necessary to allow a short range interaction to be carried out in a systematic way over a long enough time period. Typical spatial extents and velocity spreads are of order mm and

cm/s respectively, making sub-micron experiments difficult. Experiments involving atoms trapped at fixed separation from a source mass surface are in this respect preferable.

Since its first experimental realization in 1995, Bose-Einstein condensation of alkali gases has become a widely growing area of research (see, for example, the 2001 Nobel lectures of Cornell, Ketterle, and Wiemann [29] or reference[30] for a recent review). Interference of atomic de Broglie waves which develop a relative phase shift due to the Earth’s gravity has been observed in vertical arrays of trapped Bose-Einstein condensed atoms [31]. The traps were located at the antinodes of a laser standing wave, with the trap well depth determined by the laser intensity.

In the following we describe a setup involving arrays of Bose-Einstein condensed atoms trapped nearby a surface at the nodes or antinodes of a laser standing wave. The traps are thus loaded with atoms in coherent superpositions of states localized at differing distances from the surface. For each potential well, the de Broglie phase of the center of mass wave function of the atoms evolves according to the interaction potential of the local environment. The wave function of atoms localized at different potential wells of the laser can accumulate a differential phase shift due to the distance-dependence of the interaction potential with the wall. The potential will generally be a superposition of the Casimir-Van der Waals potential along with other backgrounds and possibly new short-range interactions. By adequately subtracting out the Casimir interaction and other background interactions as we discuss below, significant improvements can be made over previous searches for new forces below 1 micron. In particular the improvements could be 6 to 9 orders of magnitude at 1 micron, allowing forces of 1000 to 10^6 times gravity to be detected at these distances. Such short length scales have been relatively inaccessible to tabletop torsion balance and micro-cantilever experiments due to the necessity of having nearby moving macroscopic mechanical parts and the unfavorable scaling of the gravitational force with their size.

A. Experimental Setup and Geometry

We consider $^{87}\text{Rubidium}$ atoms prepared in coherent superpositions of states localized at the nodes or antinodes of a standing wave of an infrared laser of wavelength λ_{las} . For a laser wavelength that is red de-tuned from the dominant Rubidium D2 line, the atoms are attracted to regions of high laser intensity, corresponding to trapping at the anti-nodes.

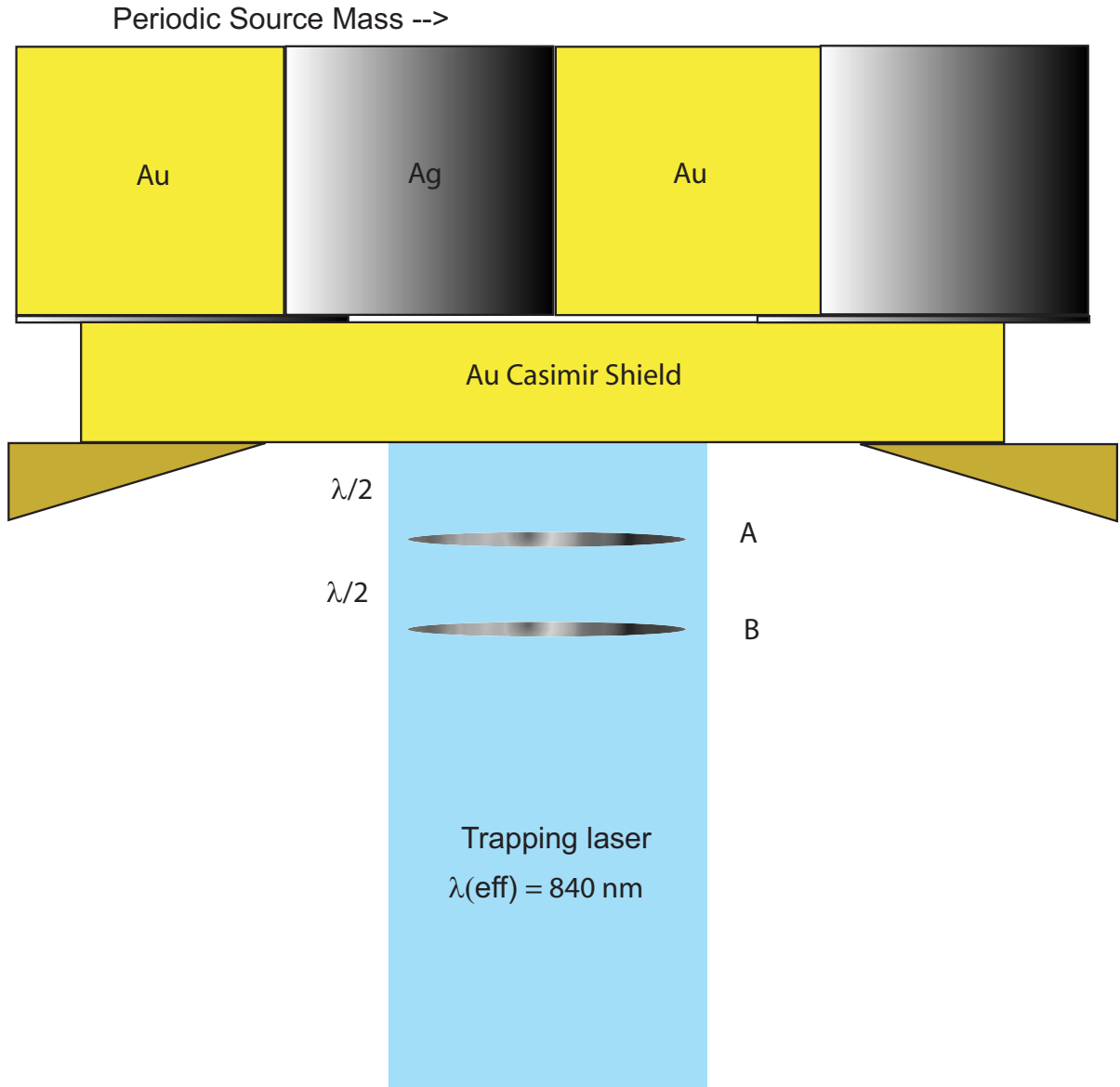


FIG. 3: Proposed experimental arrangement. The standing wave cavity formed by reflection from the Au Casimir shield is used to trap BEC atoms in the two potential wells nearest to the periodic source mass array.

On the other hand, for blue de-tuned light the potential minima occur at the nodes of the standing wave. In the first case the potential wells will be centered at distances $(\lambda_{\text{las}}/4, 3\lambda_{\text{las}}/4, \dots)$ from the surface, in the case of normal laser incidence. For blue de-tuning the wells are located at distances $(\lambda_{\text{las}}/2, \lambda_{\text{las}}, \dots)$ from the surface. The effective well separa-

tion and surface separation can readily be made larger in the case of oblique incidence at angle θ , where $k_{\perp}^2 < k^2$ and the effective wavelength determining the trap spacing becomes $\lambda = \lambda_{\text{las}} / \cos \theta$. Thus a variety of surface and well separations are attainable depending on the trap geometry. The atomic well depths can be adjusted by varying the laser intensity to overcome the atom-surface interaction potential and the Earth's gravitational field. Transverse confinement can be achieved for example through the gaussian envelope of the beam in the case of red de-tuning, or with additional laser beams.

For definiteness we consider a standing wave with an effective trap spacing of $\lambda/2 = 420$ nm. We also take the separation of the first trap and the surface to be 420 nm. The proposed geometry is illustrated in Figure 3. The laser is reflected from a 420 nm thick shield of gold. The periodic source mass consists of alternating regions of more and less dense material, for example gold and silver. Although less dense materials are preferable for the Yukawa force contrast, silver is chosen for the similarity of its diamagnetic response to that of gold to ameliorate possible problems with magnetic backgrounds. The source masses are taken to be 100 microns wide by 100 microns deep by 10 microns tall. The source mass can be moved as a whole laterally by a piezo-electric device over several hundreds of microns. To reduce temperature changes in the Casimir shield as the source mass moves, a very small space is left open directly behind the shield. We consider a population, by $\sim 10^6$ atoms, of the first two potential wells closest to the surface, denoted by A and B, respectively. The atoms will be spread out in a pancake-like configuration with a transverse extent of a few microns. The de Broglie phase of the wave function localized at the first well (A) will evolve more rapidly than that of the wave function at the second (B) due to the atom-surface interaction potential. After an interrogation time of 1-10s, the laser intensity can be rapidly turned down, allowing the wave-packets to escape, spread out, and overlap spatially. The resulting interference pattern can then be detected using optical fluorescence. If the accumulated phase difference is due to a Yukawa-type interaction with the surface, the phase difference will change depending on whether a silver or gold section of the source mass is positioned behind the Casimir shield. As the source mass is scanned behind the shield, the phase difference accumulated in a series of measurements will display a periodic behavior as the regions of more or less dense material are moved laterally behind the shield. On the other hand, the Casimir-Polder interaction will be largely the same due to the gold Casimir shield. Also, any patch fields that contribute to the interaction can be rejected

as a common mode. The magnitude of the Casimir-Polder interaction at 420 nm is some 8 times the gravitational interaction with the Earth. Due to its gigantic magnitude, it is crucial then to consider the finite-thickness corrections to the Casimir potential to estimate the potential reach of the experimental setup.

B. Sensitivity

Scaling. We compute the difference in the frequency at which the de Broglie phase evolves for adjacent populated wells of the laser near the surface due to a Yukawa-type potential of strength α and range λ . Taking the thickness of the source masses to be r and $2r$ and the atom-wall separation to be r , the potential difference can be roughly approximated as

$$\delta V(r) \sim 2\alpha G_N m \rho r \delta r \quad (11)$$

where we consider a Yukawa potential of range $\lambda \sim r$ and take $\delta r \sim r$, so that we have

$$\delta V(\lambda) \sim 2\alpha G_N m \rho \lambda^2. \quad (12)$$

Here m denotes the mass of an individual atom. For example, taking Rubidium-87 and a gold wall, the corresponding frequency shift for $\lambda = 1\mu\text{m}$ is $1.5\alpha \times 10^{-10}$ Hz. To obtain a more precise estimate, we numerically integrate the Newtonian plus Yukawa potential.

With $\sim 10^6$ atoms in the condensate, we estimate the minimal detectable phase shift per shot as 10^{-3} radians. For a conservative estimate of 1 s interrogation time, the minimal resolvable frequency shift is 1.6×10^{-4} Hz. This corresponds to an acceleration sensitivity of roughly 10^{-7} g, where g is the acceleration of the Earth's gravitational field at the surface, where we again take a trap spacing of $\lambda/2 = 420$ nm. Ultimately, an improvement could be obtained by an averaging over 10^4 shots, allowing the phase shift to be detected at the 10^{-5} level. This along with increasing the interrogation time to 10 s yields a minimal detectable frequency shift of 1.6×10^{-7} Hz, corresponding to an acceleration sensitivity of order 10^{-10} g. Obtaining larger interrogation times may be difficult due to loss of coherence from collisions or laser instability [32]. In the following we assume a sensitivity of 1.6×10^{-4} Hz. Also, the systematic effects we consider in the following sections are not generally problematic at this level, however may be more challenging for a measurement with 10^{-7} Hz sensitivity as will be discussed.

Using this minimal detectable frequency shift and the numerical results for the Yukawa potential, we generate a plot of the alpha-lambda reach in Figures 1 and 2. Such an experiment is particularly favorable in the sub-micron length scales, where macroscopic cantilever and torsion balance experiments become increasingly more challenging.

For the geometry described above with a BEC-surface separation of 0.42 microns and well separation of 0.42 microns, we evaluate the frequency shift of the potential wells due to a Yukawa potential of strength α . For lambda of $1\mu\text{m}$, we find $1.2 \times 10^{-10}\alpha$ Hz for the frequency shift, allowing alpha of $\sim 10^6$ to be probed. A plot of the projected sensitivity on alpha-lambda space appears in Figures 1 and 2 as a solid green line. We also indicate the projected improvement possible with the sensitivity taken to the 10^{-7} Hz level as a solid red line. In Figures 1 and 2, the green curve is calculated for a surface separation, trap spacing, and shield thickness of 420 nm with 1 second interrogation time and a single shot. In Figure 2 the red curve is also computed at a well separation, surface separation, and shield thickness of 420 nm. The red line in Figure 1 has been computed for a shield thickness, trap spacing, and surface separation scaled from 420 nm to 600 nm. Here we assume 10 seconds of interrogation time and average over 10^4 shots, corresponding to 10^{-7} Hz sensitivity. The larger scale of 600 nm becomes advantageous for measurements near $\lambda = 1\mu\text{m}$ as it can better suppress the Casimir background. We note that for these geometries the sensitivity levels off above 1 times gravity at large lambda. By scaling the geometry and trap spacing together, the estimated sensitivity roughly follows Eq.(12) so that 1 \times gravity is achievable at ~ 30 microns. These larger length scales are also accessible by upcoming micro-cantilever or torsion oscillator experiments. Therefore in figures 1 and 2 we have emphasized the reach at the micron scale and below.

C. Systematics

1. Casimir Background

Finite Thickness and Conductivity. The frequency shift due to the bare Casimir force is quite large (on the order of 8 kHz). However, in the case of infinite conductivity, the *differential* frequency shift between regions of metal of varying thickness is zero. In practice, the finite conductivity of the metal as well as its finite thickness has to be taken into account.

It was shown in reference [7] for the case of two metal walls that the differential Casimir background due to differences in thickness rapidly dominates the Yukawa force as thickness and plate separation decreases, thus making measurements of gravitational strength Yukawa forces difficult below a few microns. The geometry studied consisted of a semi-infinite probe mass of finite conductivity separated by a distance D from a finite conductivity source mass of thickness D . The result for the Casimir force and a gravitational strength Yukawa force of range D was then compared to the case source mass thickness $2D$. It was shown that the differential Casimir background due to differences in thickness becomes comparable to the differential Yukawa force at distances of about 3 microns and rapidly dominates the Yukawa force below this length scale. In this work we show that by replacing the metal probe mass with a dielectric, or with an atom in particular, the differential Casimir force is considerably smaller, making the domination over the Yukawa potential less severe at sub-micron lengths. Following references [7], [33] we employ a reflection-based model for computing the Casimir force between two walls. We obtain similar results to reference [7] for metallic walls. Also, we obtain a reduction factor η_F , (defined precisely in reference [33]) which describes the reduction of the Casimir force at small separations and for finite conductivity, that agrees well with the results of that reference in the case of semi-infinite walls. The parameter η_F is defined as

$$F_C = \eta_F F_P \quad (13)$$

where F_P is the perfect conductor result. The integral expression

$$\eta_F = \frac{120}{\pi^4} \int_0^\infty dK K^2 \int_0^K d\Omega \sum_p \frac{r_p^2}{e^{2K} - r_p^2} \quad (14)$$

gives η_F in terms of the reflection amplitudes r_p which can depend on the polarization, conductivity, frequency, and wall thickness [33]. Here $K = \kappa L$ and $\Omega = \omega \frac{L}{c}$ are the wavenumber and frequency measured with respect to the cavity length L .

The Casimir force between the mirrors can be expressed in terms of the imaginary part of the dielectric function of the walls. For metallic walls, the dielectric function is

$$\epsilon(i\omega) = 1 + \frac{(\omega_p)^2}{\omega(\omega + \gamma)}$$

where we assume a Drude model for the metals, and ω_p and γ are the plasma frequency and relaxation frequency, respectively. The magnitude of the Casimir force changes rapidly as the length scales of thickness and separation approach the plasma wavelength λ_p . The

expression for the reduction factor η_F which describes the fraction of the perfect metal Casimir result can be written as an integral over all frequencies and wavenumbers. In particular, the low-frequency response of the dielectric function of metals diverges as $\omega \rightarrow 0$. By replacing one of walls with a dielectric ϵ , the low-frequency response becomes weaker and contributes less to the Casimir force. As a consistency check, we evaluate the expression for a dielectric wall and metal wall using both the reflection model of reference [33] and by numerically integrating the zero-temperature Lifshitz result directly[34]. The two numerical calculations agree to a part in 10^5 . After demonstrating the equivalence of the two models for the semi-infinite case of dielectric and metal walls, we proceed with the reflection model to study the finite thickness dependence. We find the result is less sensitive to the thickness of the source metal, which improves the situation considerably for new force detection below $3 \mu\text{m}$. The reduction factor for the Casimir Force η_F for the two walls is computed for the case of wall thickness D and $2D$, for wall separation L . We define the quantity

$$\Delta\eta = \frac{\eta_F^{(2D,L=D)} - \eta_F^{(D,L=D)}}{\eta_F^{(D,L=D)}} \quad (15)$$

which expresses the fractional differential Casimir force for the source walls of different thickness. We list a table of values of $\Delta\eta$ for probe walls of metal and dielectric materials below. We also note that the interaction between two dielectric walls is much more sensitive to their thickness, due to the lack of screening present in metals. For example, we find $\Delta\eta$ can be as large as 1 percent for $D = 1 \mu\text{m}$ and $\epsilon = 10$, which compares rather poorly with the metal-dielectric case.

To achieve the limit of the atom-wall interaction, we consider rarifying the dielectric medium. This technique was used by Lifshitz to derive the individual atomic Van der Waals potential. We also add the dominant resonance for Rubidium D2 line. The dielectric function satisfies

$$\epsilon(i\omega) = 1 + 4\pi n\alpha(i\omega)$$

where α is the dynamical polarizability and n is the number-density of atoms. Considering the dominant D2 line at 780 nm with an oscillator strength of nearly 1, we approximate the polarizability as

$$\alpha(i\omega) = \frac{\omega_0^2 \alpha_0}{\omega_0^2 + \omega^2}.$$

The role of the parameter $\epsilon(0) - 1$ is now played by the quantity $4\pi n\alpha_0$. For ^{87}Rb , we have $\alpha_0 = 2.7 \times 10^{-23} \text{ cm}^3$, and even for a high number density of order $n \sim 4 \times 10^{16} \text{ cm}^{-3}$ we

TABLE I: Estimates for the differential Casimir force between a gold source mass of thickness D versus 2D, and a semi-infinite probe mass of varying materials. Smaller values indicate less sensitivity to the differential thickness.

D (μm)	$\Delta\eta_{\text{metal-metal}}$	$\Delta\eta_{\text{metal-dielectric}}$	$\Delta\eta_{\text{metal-dielectric}}$
		$\epsilon = 100$	$\epsilon = 1.001$
.1	9×10^{-5}	3×10^{-5}	2×10^{-5}
.3	5×10^{-6}	1×10^{-9}	9×10^{-11}
.6	2×10^{-6}	1×10^{-10}	4×10^{-12}
1	8×10^{-7}	1×10^{-10}	4×10^{-13}

obtain $\epsilon(0) - 1$ of $\sim 10^{-5}$, indicating even more favorable scaling of $\Delta\eta$ than shown in the Table for 10^{-3} .

It remains to estimate the minimal detectable alpha due to a Yukawa potential limited by the differential Casimir force. The Casimir potential due to the atom at distance r from an infinitely conducting surface can be written

$$U_C = -\frac{3\hbar c \alpha_0}{8\pi} \frac{1}{r^4}. \quad (16)$$

In practice we expect corrections due to the finite conductivity and the dynamical polarizability of the atom. The finite conductivity correction is less than a factor of 2 reduction for the length scales of interest. The equation (16) is strictly valid in the limit of large separation, at length scales greater than $\lambda/2\pi$ where now λ is the wavelength which contributes to the atom's polarizability. For lengths below this scale, the Casimir screening due to retardation becomes less effective and the power law changes to $1/r^3$ corresponding to the van der Waals interaction. For Rb, the dominant wavelength is 780 nm and since we are interested in length scales above 100 nm, the form in Eqn. (16) is a reasonable approximation. We now multiply the parameter $\Delta\eta$ by the difference in Casimir potentials of the wells obtained through Eq. (16) to obtain an estimate of the difference in potential shift due to the metal walls of the two thicknesses. The resulting $\Delta\delta U_C$ we compare with $\Delta\delta U_{\text{Yukawa}}$. (Here Δ sig-

nifies the change from a region of thickness D to $2D$, and δ signifies the different locations of the condensates A and B. In Figure 4 we abbreviate both by $d = \Delta\delta$.) In order to illustrate the scaling, we consider a set-up with equal length D for λ , the well spacing, and the atom-wall separation, and compare regions of metal thickness D and $2D$. We display the results in Figure 4 and take a Yukawa force of gravitational strength, $\alpha = 1$. For comparison we include as a dotted line the estimate adapted from reference [7] which illustrates the scaling of the differential $\alpha = 1$ Yukawa and Casimir forces for a metallic probe wall in place of the atoms. The situation for the atom-wall setup is more optimistic than that of the metallic wall-wall setup (shown in Fig [5] of reference [7]) by several orders of magnitude between 200 nm and 3 microns. In Figure 4 there are two separately labelled vertical axes shown since the atom-wall Yukawa detection limit due to the differential Casimir background is determined by the ratio of the potential differences, whereas for the metallic wall-wall system the relevant quantity is the ratio of the forces. This does not prevent a direct comparison of the α - reach of the two systems however. For example, we see from the figure that α of 10^3 can be reached at .6 microns in the metal-atom case and at about 1.5 microns in the metal-metal case.

Temperature Effect. The temperature dependence of the Casimir force becomes quite weak for low temperatures and small separations. However, it is important to estimate the temperature-dependent contribution since the full magnitude of the Casimir force is so large. A perturbation approach has been developed in reference [35]. We employ the parallel metal plate expression valid for separations below 2 microns as a function of temperature T :

$$\Delta\eta_F(T) = \left(\frac{4}{3t^5} + \frac{2\delta}{a} \frac{15}{\pi^2} \frac{3\zeta(3)}{t^4} \right) \Delta t \dots, \quad (17)$$

where $t = T_{\text{eff}}/T$, $T_{\text{eff}} = \hbar c/2ak_B$, $\delta = \lambda_p/2\pi$, and a is the plate separation. Taking a separation of $a = 840$ nm, a gold surface of $\lambda_p = 136$ nm, we find for a room-temperature of 295 K, the parameter $t = 4.6$. This amounts to a fractional change in the Casimir force $\Delta\eta_F = .0012\Delta t$ and writing Δt as $t\frac{\delta T}{T}$, we have

$$\Delta\eta_F(295\text{K}) = 0.0055 \times \frac{\delta T}{T} \dots \quad (18)$$

which can be a significant effect. If the entire reflecting surface changes temperature by 10^{-6} K during the measurements, the frequency shift is at the 10^{-7} level. For the proposed initial parameters the sensitivity to wall temperature is at the \sim mK level. However, most

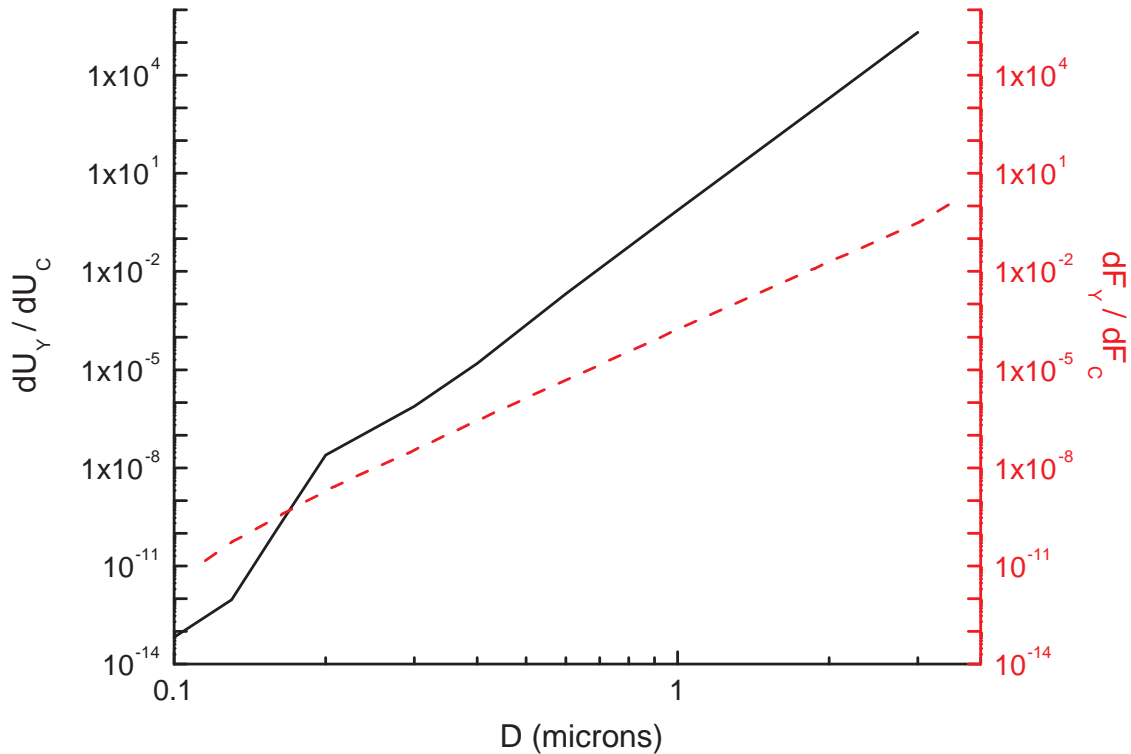


FIG. 4: Estimate for the Yukawa detection limit due to Casimir-Van der Waals background for Yukawa range $\lambda = D$ and strength relative to gravity $\alpha = 1$ is shown as the black solid line for the atom-wall system. The well spacing and atom-wall separation are also D , and we compare regions of metal thickness D and $2D$. The metal-metal case studied in reference [7] is shown as a red dotted line for comparison.

of the Casimir force results from the wall material closest to the atom, which we suggest to take as a shield of uniform material, and have the pattern of varying density source masses separated from this material by a small distance to prevent heating upon motion. Even though a small temperature gradient could be supported across the shield wall, it is unlikely that the shield surface temperature will vary periodically with the source mass density, as the two are not in direct thermal contact. A periodic temperature gradient in the source mass distribution itself changes the expected Casimir force very little, as its effect comes in only at the level of $\Delta\eta$ due to the thickness of material calculated in the previous section. As an additional handle, the temperature of the surfaces can be controlled externally to

quantify the effect experimentally. Also, decreasing the temperature improves the situation considerably, yielding a sensitivity to a full wall temperature change of $\sim 10^{-3}$ K at 77 K and only to ~ 10 K at liquid helium temperature for frequency shifts of 10^{-7} Hz.

Isotope Effect. A unique feature of atomic systems in contrast to macroscopic objects is that the electrical properties and mass of the atom can be toggled in a precise way by taking advantage of other stable atomic isotopes. For example, by using ^{85}Rb , and comparing to an experiment done with ^{87}Rb , one expects the force to change at the 10^{-2} level, while the Casimir force changes only at the $10^{-4} - 10^{-5}$ level. To verify this claim, we compute the Casimir force for each isotope according to the Lifshitz model, and simply change the wavelength of the dominant transition from 780 nm to 780.1 nm. Although this technique decreases the sensitivity to alpha by 2 orders of magnitude, it may be useful for doing measurements at around 100 nm separation from the surface, where the differential Casimir force rapidly dominates over the Yukawa force due to the finite plasma wavelength of the metal.

2. Magnetic and Other Backgrounds

Magnetic Susceptibility. Local magnetic field gradients can be caused by the variation in magnetic susceptibility of the two source mass materials. For a background magnetic field, e.g. from the Earth, the induced magnetic dipole moment in the materials produces a field which varies in proximity to the two materials. The induced magnetization in a paramagnetic or diamagnetic material satisfies

$$\vec{M} = \frac{\chi_m}{(1 + \chi_m)\mu_0} \vec{B}$$

Now the induced field due to the magnetized materials we roughly approximate using the expression for a magnetized sphere

$$B(z) = \frac{2\mu_0 M a^3}{3z^3} = \frac{2\chi_m}{(1 + \chi_m)} B_0 \frac{a^3}{3z^3}$$

where a is the sphere radius and \vec{B}_0 is the background magnetic field responsible for the induced magnetization. We find the differential field to be

$$\begin{aligned} \Delta B_z(z) &= \frac{2\Delta\chi}{(1 + \chi)} B_0 \frac{a^3}{z^3} \left(\frac{\Delta z}{z} \right) \\ &\sim \frac{2}{100} \Delta\chi B \end{aligned}$$

where in the last line we assume $\Delta z = 420$ nm and we take the radius to be $a = 50\mu\text{m}$. Silver and Gold are both diamagnetic, with a differential susceptibility of $.6 \times 10^{-5}$. We estimate $\Delta B \sim 10^{-7}B$. The frequency shift due to magnetic fields for Rubidium is 1.4 MHz/Gauss, so to obtain 10^{-4} Hz resolution only requires a magnetic field shielding of $B_0 < 1$ mG. One can further alleviate the constraints on background magnetic fields by choosing materials that have more similar magnetic susceptibility either in pure form or through selective doping. Although not problematic for the initial proposed parameters, extending the Yukawa sensitivity down to the $\sim 10^{-7}$ Hz will require more extensive magnetic shielding or precisely tailored alloy or doped materials.

Gravity as a background. Although heavy nearby objects can be easily detected, this is not expected to be problematic since they in general cannot exhibit the periodicity of the source mass pattern. We note that in order to avoid acquiring a differential background signal at the 10^{-7} Hz level due to the gravitational attraction of the proof masses themselves (which is only power-law suppressed and so remains significant at distances much greater than the λ of interest below $1\mu\text{m}$), it is necessary to limit the vertical extent of the proof masses to be less than approximately $100\mu\text{m}$.

Finally, we list a number of other systematic backgrounds which are not expected to be problematic due to common-mode rejection. They include patch field effects on the surface of the reflecting metal shield, the roughness of the surface of the shield, the background Earth's gravitational field.

We conclude this section with a table summarizing the expected frequency shifts of selected systematics as they compare to the Yukawa signal.

V. DISCUSSION

The search for short-distance modifications to Newtonian gravity has rapidly expanded over the past seven years. We have illustrated several possible examples of sub-millimeter physics that may occupy a vast amount of still unexplored parameter space. We have also described an experimental technique involving interference from arrays of Bose-Einstein condensed atoms that could extend the search by several orders of magnitude below a micron. Such techniques, if successful, allow access to an area of phase space that is complementary to the super-micron reach of upcoming torsion oscillator and micro-cantilever experiments

TABLE II: Summary of selected systematic effects. The three backgrounds: Newtonian, Δ Casimir, and magnetic are evaluated for a surface separation, trap spacing, and shield thickness of 420 nm. Scaling these distances from 420 nm to 600 nm causes the differential Casimir signal to drop below the 10^{-7} Hz level.

Yukawa signal	
λ	Δf (Hz)
1 μ m	$1.2 \times 10^{-10} \alpha$
.6 μ m	$3.6 \times 10^{-11} \alpha$
.3 μ m	$3.4 \times 10^{-12} \alpha$
.1 μ m	$1.8 \times 10^{-15} \alpha$
Background	
Newton	6.5×10^{-9} Hz
Casimir	8283 Hz
$\Delta\eta$	7×10^{-11}
Δ Casimir	5.7×10^{-7} Hz
Magnetic	3×10^{-5} Hz $\times \frac{\Delta\chi}{10^{-6}} B$ (mG)

and could lead to exciting discoveries.

VI. APPENDIX

In this appendix we estimate the range and strength of forces due to gauged baryon number in the bulk. The mass of a macroscopic object is roughly in proportion to the number of baryons, and the expected ratio of the gauge to gravitational forces takes the form

$$\alpha = \frac{F_{gauge}}{F_{grav}} = \frac{g_4^2}{4\pi G_N m_p^2} \quad (19)$$

where m_p is the mass of the proton. As discussed in the text, we take the 4+n dimensional gauge coupling as $g_{4+n}^2 = \Lambda^{-n} \mathcal{O}_{4+n} \rho$, where Λ is the ultraviolet cutoff scale and $\mathcal{O}_d = \Omega_{(d-1)} / (2\pi)^d$ is the 1-loop suppression factor. If the coefficient ρ is $\mathcal{O}(1)$, this signifies strong coupling at the scale Λ in the 4+n dimensional theory, as loop effects become comparable

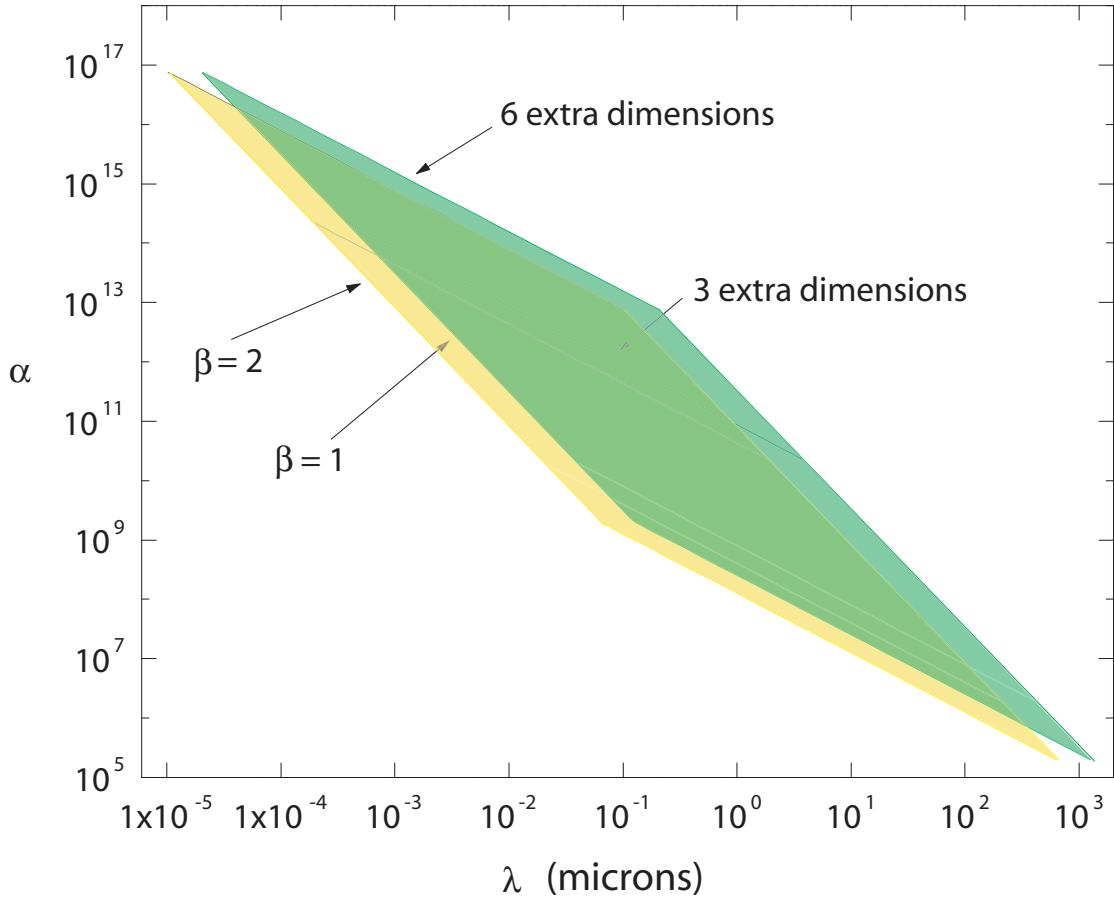


FIG. 5: Interaction strength and range for gauged Baryon number in the bulk. $\alpha = 1$ corresponds to a force of Newtonian gravitational strength. For illustration, the case of $\beta = 1$ is shown as the green right-most parallelogram and $\beta = 2$ is shown in yellow. The ranges for strong and weak coupling in 3 and 6 extra dimensions are shown. The upper limit shown for the strong-coupling region in the case of 3 extra dimensions terminates at smaller alpha as shown. The weak-coupling lower boundary is identical for both cases.

to tree-level. Using $\Omega_{d-1} = 2\pi^{d/2}/\Gamma(\frac{d}{2})$, we find the familiar 4-dimensional loop factor $\mathcal{O}_4 = 16\pi^2$. For three extra dimensions the factor becomes $\mathcal{O}_7 = 15 \cdot 8\pi^4$ and for six extra dimensions $\mathcal{O}_{10} = 12 \cdot 1024\pi^5$. The effective 4-d gauge coupling satisfies

$$\begin{aligned} \frac{1}{g_4^2} &= \frac{V_d}{g_{(4+n)}^2} \\ &= \left(\frac{M_4}{M_*}\right)^2 \frac{1}{V_{n-d} M_*^{n-d}} \frac{1}{\mathcal{O}_{d+4} \rho} \left(\frac{\Lambda^d}{M_*^d}\right) \end{aligned}$$

where in the second line we have assumed that the gauge bosons propagate in $d \leq n$ of the extra dimensions. For definiteness, we consider the case of gauge bosons living in all extra dimensions ($n=d$), and the expression simplifies to

$$g_4^2 = \left(\frac{M_*^2}{M_4^2}\right) \mathcal{O}_{n+4} \cdot \rho\left(\frac{M_*^n}{\Lambda^n}\right). \quad (20)$$

so then the ratio of forces becomes

$$\alpha = \frac{g_4^2}{4\pi} \frac{1}{G_N m_p^2} \quad (21)$$

$$= \left(\frac{M_*^2}{m_p^2}\right) 25 \frac{\mathcal{O}_{n+4} \cdot \rho\left(\frac{M_*^n}{\Lambda^n}\right)}{4\pi}. \quad (22)$$

The factor of 25 appears as the square of the approximate ratio between $1/\sqrt{G_N}$ and the reduced Planck mass. For M_* of order TeV, already the force becomes ~ 1 million times gravity. If the gauge symmetry is spontaneously broken by a scalar field χ obtaining a vacuum expectation value $\langle \chi \rangle$, the resulting mass of a gauge particle A_μ becomes

$$m_A = g_4 \langle \chi \rangle. \quad (23)$$

Here again we assume that χ condenses on a brane other than our own. It was shown in reference [24] that forces mediated by bulk gauge fields can be exponentially weaker than gravity if the bulk gauge symmetry is spontaneously broken on our brane.

We parameterize the vacuum expectation value of χ as

$$\langle \chi \rangle = \beta \cdot \Lambda \quad (24)$$

where beta is a numerical coefficient of order 1, so that the Compton wavelength is written

$$\lambda_A = \frac{1}{\mathcal{O}_{n+4} \cdot \rho} \frac{M_4}{M_*^2} \frac{1}{\beta} \frac{\Lambda^{n/2}}{M_*^{n/2}} \quad (25)$$

If the scale Λ is somewhat smaller than M_* , the Compton wavelength becomes shorter and the strength α_g increases. For example, if one imagines new physics arising from string theory at scale M_s , we have the relation

$$\frac{M_s^{2+n}}{g_s^2} \sim M_*^{2+n}$$

so that

$$M_s = M_* (g_s^2)^{1/(2+n)} \leq M_*. \quad (26)$$

where we have identified the Lagrangian

$$\int d^4x \sqrt{-g} \mathcal{R} M_*^{2+n} V_n = \int d^4x \sqrt{-g} \mathcal{R} M_4^2 \quad (27)$$

with a Type I string Lagrangian [4]

$$\int d^4x \frac{1}{g_s^2} M_s^{2+n} V_n \sqrt{-g} \mathcal{R}.$$

If Λ is associated with physics at the string scale, it is possible the coefficient β is greater than 1.

In order to illustrate the phase space encompassed by these forces, in Fig. 1 we plot α versus λ_A , where for simplicity we set $\Lambda = M_*$ and we vary the parameter ρ from $1/(10 \times \mathcal{O}_{d+4})$ for weak coupling, to 1 for strong coupling. We vary M_* from 1 TeV to 100 TeV, and show β between 1 and 2. For smaller β , the predicted region can be extended horizontally to the right until conflicting with experimental observation.

Finally we note the gauge force we discuss is due strictly to the zero-mode, and therefore its range is not strongly limited by the size of the extra dimensions. In the case that any of the extra dimensions has a large enough compactification radius, the lightest KK modes of the gauge particles may also make a contribution, though we do not include this explicitly in Figures 1 and 2.

Acknowledgments

We are indebted to Mark Kasevich who contributed immensely to the development of this work. We also thank Ignatios Antoniadis, Blas Cabrera, and Vladan Vuletic for useful discussions. This work is supported by grant NSF-PHY-9870115.

- [1] S. Dimopoulos and G.F.Giudice, Phys.Lett. **B379**, 105-114 (1996).
- [2] I. Antoniadis, S. Dimopoulos, G. Dvali Nucl.Phys. **B516**, 70-82 (1998).
- [3] Nima Arkani-Hamed, Savas Dimopoulos, and Gia Dvali. Phys.Lett. **B429**, 263-272 (1998).
- [4] Ignatios Antoniadis, Nima Arkani-Hamed, Savas Dimopoulos, Gia Dvali, Phys.Lett. **B436**, 257-263 (1998) ,hep-ph/9804398.

- [5] Nima Arkani-Hamed, Savas Dimopoulos, and Gia Dvali. Phys.Rev. **D59** ,086004 (1999), hep-ph/9807344.
- [6] Raman Sundrum, JHEP 9907:001,1999.
- [7] Joshua C. Long, Allison B. Churnside, John C. Price, Proceedings of the Ninth Marcel Grossmann Conference (Rome, 2-8 July 2000), hep-ph/0009062.
- [8] C. D. Hoyle, U. Schmidt, B. R. Heckel, E. G. Adelberger, J. H. Gundlach, D. J. Kapner, H. E. Swanson, Phys.Rev.Lett. **86** , 1418-1421 (2001) .
- [9] J. Chiaverini, S. J. Smullin, A. A. Geraci, D. M. Weld, A. Kapitulnik , Phys.Rev.Lett. **90**, 151101 (2003).
- [10] Joshua C. Long, Hilton W. Chan, Allison B. Churnside, Eric A. Gulbis, Michael C. M. Varney, John C. Price , Nature 421, 922 - 925 (2003).
- [11] For a recent review see Joshua C. Long and John C. Price, to be published in Comptes Rendus Physique hep-ph/0303057.
- [12] G. F. Giudice and R. Rattazzi, Phys.Rept. **322**, 419-499 (1999), hep-ph/9801271.
- [13] E. Fischbach, D. E. Krause, V. M. Mostepanenko, M. Novello, Phys.Rev. **D64** , 075010 (2001).
- [14] J.K. Hoskins *et al.*, *Phys. Rev.* **D32** (1985) 3084.
- [15] S. Lamoreaux, Phys.Rev.Lett. **78**,5 (1997).
- [16] G. Veneziano and T. Taylor, *Phys. Lett.* **B213** (1988) 450.
- [17] David B. Kaplan, Mark B. Wise, JHEP 0008, 037 (2000).
- [18] T. Damour, A. M. Polyakov, Nucl.Phys. **B423**, 532-558 (1994).
- [19] A. Kehagias and K. Sfetsos, Phys.Lett. **B472**, 39-44 (2000) , hep-ph/9905417.
- [20] E.G.Floratos and G.K. Leontaris, Phys.Lett. **B465**, 95-100 (1999), hep-ph/9906238.
- [21] Steen Hannestad and Georg G. Raffelt, Phys.Rev.Lett. **88** ,071301 (2002).
- [22] G.R. Dvali, G. Gabadadze, M. Kolanovic, and F. Nitti, Phys.Rev. **D64** 084004 (2001).
- [23] Nima Arkani-Hamed and Savas Dimopoulos,Phys.Rev. **D65**, 052003 (2002), hep-ph/9811353.
- [24] Gia Dvali, Gregory Gabadadze, Massimo Porrati, Mod.Phys.Lett. **A15**, 1717-1726 (2000), hep-ph/0007211.
- [25] Schuyler Cullen, Maxim Perelstein, Phys.Rev.Lett. **83**, 268-271 (1999).
- [26] S.Chu, S.Cohen-Tannoudji, and W.Phillips, Nobel lectures 1998.
- [27] A. Peters, K.Y. Chung, and S. Chu, Metrologia, 2001, **38**, 25-61.
- [28] J.M. McGuirk, G.T. Foster, J.B.Fixler, M.J.Snadden, and M.A.Kasevich, Phys.Rev. **A65**

033608 (2002).

- [29] E.Cornell, W.Ketterle, and C.Wiemann, Nobel lectures 2001.
- [30] Anthony J. Leggett, Rev.Mod.Phys.**73**,307(2001)
- [31] B.P.Anderson and M.A.Kasevich, Science 282, 1686 (1998).
- [32] Mark Kasevich, private communication.
- [33] Astrid Lambrecht, Serge Reynaud, Eur.Phys.J. D8, 309-318 (2000) quant-ph/9907105.
- [34] L.D.Landau and E.M. Lifshitz. Statistical Physics vol. 2, ch 13.
- [35] B. Geyer, G.L. Klimchitskaya, V.M.Mostepanenko Phys. Rev. **A65**, 062109 (2002).